THE JOURNAL OF PHYSICAL CHEMISTRY C
A JOURNAL OF THE AMERICAN CHEMICAL SOCIETY

pubs.acs.org/JPCC

Article

Accelerated Data-Driven Discovery and Screening of Two-Dimensional Magnets Using Graph Neural Networks

Published as part of The Journal of Physical Chemistry C virtual special issue "Machine Learning in Physical Chemistry Volume 2".

Ahmed Elrashidy,* James Della-Giustina, and Jia-An Yan*

Cite This: *J. Phys. Chem. C* 2024, 128, 6007–6018

Read Online

ACCESS | Metrics & More | Article Recommendations | Supporting Information

ABSTRACT: In this study, we employ graph neural networks (GNNs) to accelerate the discovery of novel 2D magnetic materials which have transformative potential in spintronic applications. Using data from the Materials Project database and the Computational 2D materials database, we train three GNN architectures on a dataset of 1190 magnetic monolayers with energy above the convex hull (E_{hull}) less than 0.3 eV/atom. Our Crystal Diffusion Variational Autoencoder generates 11,100 candidate crystals. Subsequent training on two Atomistic Line GNNs achieves 93% accuracy in predicting magnetic monolayers and a mean average error of 0.039 eV/atom for E_{hull} predictions. After narrowing down candidates based on magnetic likelihood and predicted energy, constraining the atom count in the monolayers to five or fewer, and performing dimensionality checks, we identified 190 candidates. These are validated using density-functional theory to confirm their magnetic and energetic favorability, resulting in 167 magnetic monolayers with E_{hull} < 0.3 eV/atom and a total magnetization of ≥0.5 μ_B. Our methodology offers a way to accelerate the exploration and prediction of potential 2D magnetic materials, contributing to the ongoing computational and experimental efforts aimed at the discovery of new 2D magnets.

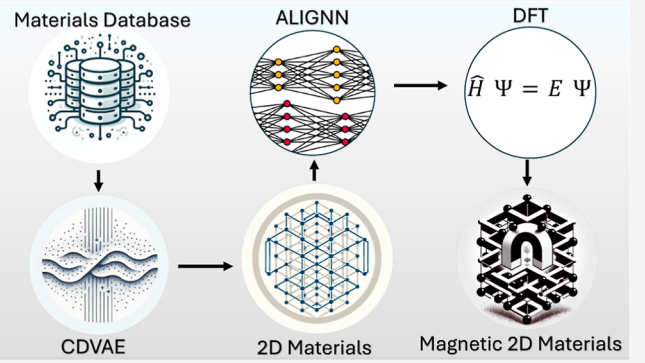

INTRODUCTION

Data-driven approaches have recently had a significant impact on discovering novel materials. Many methodologies in data-driven studies of materials utilize high-throughput density-functional theory (DFT) calculations, leading to the development of multiple databases of materials in one, two, and three dimensions. Prominent examples are the Materials Project (MP) database,[1] the Joint Automated Repository for Various Integrated Simulations (JARVIS),[2] the Open Quantum Materials Database (OQMD),[3,4] the Computational 2D Materials Database (C2DB),[5,6] and the Computational 1D Materials Database (C1DB),[7] among others. More recently, the fusion of DFT and machine learning (ML) techniques has become an invaluable tool for discovering new materials and understanding the properties of existing ones. Specifically, the introduction of ML approaches has offset some of the need for the expensive computational resources that DFT calculations often demand.[8] One notable example of the efficiency of this hybrid approach is the experimental realization of new ultra-incompressible materials found through a combination of DFT calculations and Bayesian optimization.[9] This approach has also been expanded to utilize a stacked model that combines multiple ML models coupled with high-throughput DFT to discover Fe-based bimetallic chalcogenides.[10]

High-throughput methods and ML models are also making progress in discovering and studying 2D materials.[11] A combination of ML models and DFT calculations were used to explore the structural and thermodynamic stability of 2D materials, in addition to screening functional 2D materials for energy conversion and storage.[12−14] Moreover, a symmetry-based approach has been devised to screen for all thermodynamically stable combinations of binary and ternary 2D materials, and high-throughput DFT calculations were utilized in discovering 2D superconductors.[15,16]

Historically, the realization of a 2D magnet has been deemed infeasible due to the Mermin−Wagner Theorem unless a magnetic anisotropy is present in the system.[17] The first indication of the existence of intrinsic 2D magnetism down to

Received: October 31, 2023
Revised: March 12, 2024
Accepted: March 15, 2024
Published: April 1, 2024

the monolayer limit was demonstrated through the discovery of antiferromagnetic (AFM) order in $FePS_3$.[18] Following the discoveries of ferromagnetic (FM) order in monolayer CrI_3,[19] $Cr_2Ge_2Te_6$,[20] Fe_3GeTe_2,[21] $CrBr_3$,[22] and other materials have attracted much interest in this class of 2D materials.

The discovery of new 2D magnets has become a very active field of research due to its potential in developing the next generation of nanoelectronic devices encompassing spintronic applications.[23] In fact, several experimental observations of room-temperature magnetism could mean that practical applications that capitalize on this class of materials may not be far from becoming a reality.[24−29] Nonetheless, 2D magnets are mostly not air-stable, which presents a challenge for their adoption in potential applications.[30] Another important long-standing challenge is the realization of semiconducting magnets with critical temperatures above room temperature.[31] Additionally, many 2D magnets exhibit interesting quantum phenomena such as superconductivity,[32] spin liquid states,[33,34] and topological phases.[35−38] Consequently, this class of materials presents itself as a playground for quantum phenomena and strongly correlated effects, in addition to its numerous potential applications. As a result, many studies have been devoted to high-throughput and ML approaches to discover new 2D magnets.

One of the notable successes of these studies has been the identification of Cr_3Te_4 as a promising candidate for 2D magnetism.[39] This material has been recently experimentally synthesized and verified to be a layer-dependent ferromagnet.[40] Additionally, high-throughput calculations have been utilized to screen for 2D magnetic materials based on experimental databases,[41] predict the ground state of collinear magnetic order,[42] and search for magnetic topological 2D materials.[43] Other studies have also focused on the role of magnetic anisotropy in 2D magnets.[44−46]

Additionally, a semi-supervised ML approach was adopted to identify thermodynamically stable 2D magnets for spintronic applications.[47] The investigation of 2D magnets by means of atomic substitution has been carried out for compounds of the forms $A_2B_2Te_6$ and $A^iA^{ii}B_4X_8$ using DFT and ML.[48,49] ML approaches such as XGBoost has also proven effective in gaining a deeper physical understanding of the magnetic ordering of 2D magnets.[50,51]

Despite the success of many high-throughput and ML techniques in predicting material properties and even discovering new ones, they are often limited in how they represent materials. This is because crystalline materials often do not naturally lend themselves to traditional ML structures such as vectors and matrices. To overcome this challenge, graph neural networks (GNNs) emerge as a promising solution. Differing from traditional feed-forward multilayer perceptron neural networks, GNNs excel in processing graph-structured input.[52] Through message-passing mechanisms, GNNs can iteratively update node representations based on information from neighboring nodes and edges. This capability makes them particularly apt for material property exploration and inverse design.[53]

Herein, we have generated new 2D magnets by using the crystal diffusion variational autoencoder (CDVAE), a generative model designed for generating stable materials by learning from the data distribution of known materials.[54] Additionally, we also employ the Atomistic Line GNN (ALIGNN)[55] and the materials graph with three-body interactions neural network (M3GNet).[56]

The advantage of using diffusion models,[57,58] in comparison to elemental substitution, is that it streamlines the material generation process. These models eliminate the need to wade through countless potential stoichiometries and symmetries, adopting a data-driven approach instead. Additionally, graph-based diffusion models have shown great promise in tasks like designing inorganic crystals,[59] generating 1D and 2D materials,[60,61] producing potential superconducting materials,[62] and curating stable spintronic materials.[63]

In this work, GNNs were utilized in conjunction with high-throughput DFT calculations to methodically develop an accelerated data-driven approach for 2D magnet discovery. This was achieved through a four-step process. First, magnetic monolayers are generated by a CDVAE model. Then, the monolayers are screened through ALIGNN models in addition to charge neutrality, electronegativity, number of atoms, and dimensionality checks. Next, a symmetry-constrained relaxation is performed using M3GNet IAP (interatomic potential). Finally, further DFT relaxations and self-consistent calculations are performed to assess the magnetic properties and the thermodynamic stability of the screened monolayers.

COMPUTATIONAL METHODS

CDVAE. CDVAE generates new materials by learning from the available crystalline structures in the training data. The model does not directly use predefined chemical formulas; instead, it learns to generate crystals that are likely to be stable by identifying energy minimums and bonding preferences between different types of atoms from the data. Hence, the compositions, ratios of elements in the generated materials, and their chemical and physical properties are indirectly derived from the training data. Additionally, it incorporates stability through a noise conditional score network as the decoder of the variational autoencoder (VAE).[64] This decoder utilizes a harmonic force field to estimate the forces on atoms when their coordinates deviate from the equilibrium positions, thereby providing an important physical-inductive bias for generating stable materials. CDVAE encodes permutation, translation, rotation, and periodic invariances through SE(3) equivariant GNNs adapted with periodicity.[65] This allows CDVAE to generate valid, diverse, and realistic materials in addition to its ability to optimize physical and chemical properties in latent space.

We utilized a CDVAE model to generate magnetic monolayers, training it on the available data of magnetic monolayers from C2DB. The database consists of more than 15,000 monolayers with a multitude of properties calculated through DFT. From C2DB, we curated a dataset of 1190 monolayers by filtering only magnetic monolayers with E_{hull} less than 0.3 eV/atom. The dataset was partitioned using an 80-10-10 split, allocating 80% for training, 10% for validation, and 10% for testing. It should be emphasized that the E_{hull} cutoff value applied in this context serves not as a stability criterion but simply as a threshold for selecting training data. This value of 0.3 eV/atom was chosen to be consistent with previous work that employed CDVAE to incorporate new entries to C2DB.[60] The distribution of the energy relative to the convex hull of the training set is shown in Figure 1.

ALIGNN. This model leverages both the atomic graph structure of the material and its corresponding line graph, which is derived from the original graph by transforming each edge into a vertex. The edge set of the line graph is then constructed based on whether two edges shared a mutual

https://doi.org/10.1021/acs.jpcc.3c07246
J. Phys. Chem. C 2024, 128, 6007−6018

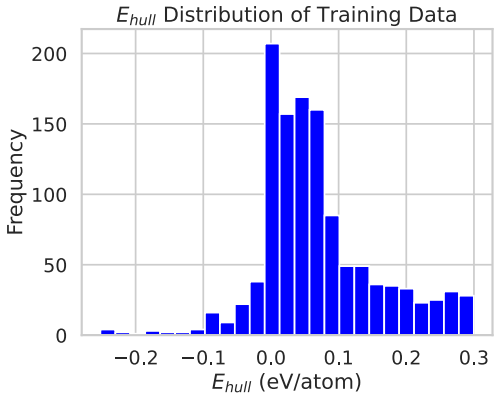

Figure 1. Distribution of E_{hull} of the 1190 training examples. The negative energies relative to the convex hull are due to monolayers that also exist in competing bulk phases with formation energies calculated using DFT + U, which can lead to an overestimation of the formation energies.[5]

vertex in the original graph; if so, they now share an edge in the line graph. By associating edges with the interatomic distances and vertices with the elemental properties of each atom in the original graph, alongside correlating edges with bond angles and vertices with interatomic bonds in the line graph, ALIGNN can capture an extensively higher degree of information. This is achieved by sequentially performing message passing on each graph and facilitating information propagation between the two.

We trained two ALIGNN architectures using a dataset of 154,718 materials from the MP database and an 80-10-10 split for training. The first model is a regression model to predict the E_{hull} of the entries, and the second is a classification model to predict magnetism.

M3GNet Relaxation. M3GNet is a GNN architecture designed to be a universal IAP for materials. It is trained on a large dataset of energies, forces, and stresses from structural relaxations performed by the MP, and is capable of predicting the properties of individual atoms as well as the overall crystal structure. M3GNet uses a three-body interaction model and is able to capture long-range interactions without the need to increase the cutoff radius for bond construction. The architecture represents the elemental information for each atom as a learnable embedding vector, making it readily extendable to multicomponent chemistries.

Force field methods have been suggested as prestructure optimizers before performing DFT calculations.[66] By utilizing the default pretrained M3GNet IAP, we conducted a symmetry-constrained relaxation of the cell shape, which is achieved by applying tensile and compressive strains within the plane of the monolayers. This allows us to approach the neighborhood of the potential energy surface minima at a fraction of the cost of DFT before performing full relaxations.

DFT Calculations. For the DFT calculations, we employed the projected augmented wave method as implemented in the Vienna ab initio Simulation Package.[67,68] We chose the Perdew−Burke−Ernzerhof (PBE)[69] formulation for the generalized-gradient approximation exchange-correlation functional (GGA). The Brillouin zone underwent sampling using a $9 \times 9 \times 1$ k-point grid mesh[70] with a 600 eV plane wave cutoff energy. This mesh size was chosen so that after M3GNet relaxations, the k-point density for the smallest lattice vector in the considered materials is 4 points/Å^{-1}.

Limiting our considerations to the ferromagnetic states, initial magnetic moments were assigned to the atoms for collinear magnetic calculations without spin−orbit coupling. Transition metal elements were initialized with a magnetic moment of 6 μ_B, while all other elements were initialized to a value of 0.5 μ_B. This intentional overestimation aims to facilitate convergence and relaxation in the accurate ferromagnetic ground state.

Each structure was fully relaxed until the Hellmann−Feynman forces on every atom were less than 2×10^{-2} eV/Å, and the energy convergence criterion reached 10^{-6} eV. For self-consistent evaluations, a more stringent energy convergence criterion of 10^{-7} eV was applied.

It is worth noting that this approach does not consider AFM order and therefore could miss energetically favorable AFM phases if present. As this work is concerned with developing an approach for accelerating 2D magnet discovery, considering AFM states that typically require increasing the size of the unit cell goes beyond our scope. Additionally, we have used PBE functionals throughout with no inclusion of a Hubbard-U correction in order to be consistent with the computational methodology of C2DB; this also allows for a more consistent energetic favorability analysis. Nonetheless, many magnetic 2D materials exhibit strongly correlated effects and are better suited for more advanced methods that account for correlation in the outer electronic shells, such as DFT + U,[71−73] dynamical mean field theory,[74] and quantum Monte Carlo.[75] These

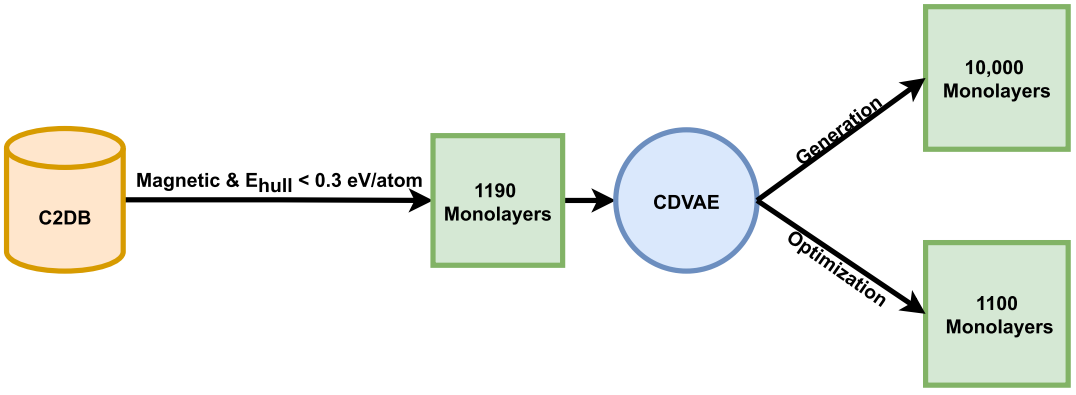

Figure 2. Outline of training CDVAE to generate 11,100 candidate monolayers for further screening.

https://doi.org/10.1021/acs.jpcc.3c07246
J. Phys. Chem. C 2024, 128, 6007−6018

methods have proven to be more accurate in describing materials manifesting strong correlation effects.[76−80]

RESULTS AND DISCUSSION

Generating 2D Magnets. In C2DB, the material properties of the greatest importance for our goal are the magnetic and thermodynamic ones. Specifically, we are interested in the energy above the convex hull (E_{hull}). The energy of the convex hull is derived from the Gibbs free energy at 0 K and 0 atm pressure by constructing the convex hull set of the normalized formation energy with respect to the number of atoms. The energy above the hull calculation provides an additional advantage over using the formation energy per atom (E_f). This advantage stems from E_{hull} assessing the energetic favorability of compounds relative to other competing phases in terms of their formation energies. Therefore, a compound's stability is inversely proportional to its energy above the convex hull; the less stable it is, the higher its E_{hull}. In many data-driven approaches to generating materials, E_{hull} has become a standard measure to assess the thermodynamic stability of the generated materials.[15,60−63,81−83]

We trained the CDVAE model to perform two tasks, generating monolayers both with and without optimization for the energy above the convex hull in latent space. The model yielded 11,100 candidate monolayers which were subsequently screened. This process to generate these monolayers is depicted in Figure 2. For reference, the distribution of the top-generated stoichiometries by CDVAE is shown in Figure 3.

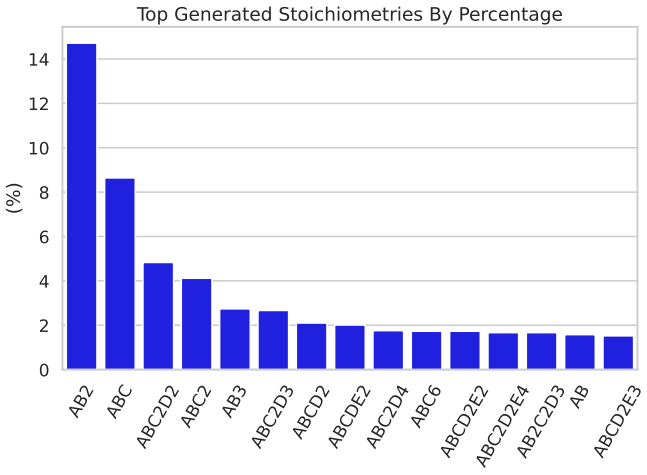

Figure 3. Distribution of stoichiometries generated by CDVAE.

The majority of the materials were generated without optimization of the E_{hull} in the latent space. This was done to increase the number of candidates since the training dataset was filtered to only contain materials within proximity to E_{hull}.

Training ALIGNN Discriminator Models. While DFT remains the gold standard in determining the properties of 2D materials, including thermal stability and magnetic properties, performing thousands of DFT calculations requires a considerable amount of time and computational resources.

This becomes a crucial factor when considering that many of the generated monolayers may not be magnetically or thermodynamically stable. Therefore, we utilized the ALIGNN models to filter candidates by their magnetic probability and thermal stability before running DFT calculations. The outline of how the ALIGNN models were utilized and the results of training are illustrated in Figure 4.

The regression model predicts E_{hull} and achieves a MAE (mean average error) of 0.028 eV/atom. We then employ transfer learning and further train the model on the monolayers in C2DB to predict the energy above the convex hull and obtain a MAE of 0.039 eV/atom. The second model is utilized to classify whether a material is magnetic, which has previously been accomplished in ALIGNN performance benchmarks by specifying a cutoff value of 0.05 μ_B for the total magnetic moment.[55] Using this strategy, the model attains an accuracy of 87.30% on the test dataset, likely due to the fact that this approach effectively classifies the data into ferromagnets or nonferromagnets. Moreover, within the same material, structural deformations through strain may be associated with a change in the magnetic order.[84−86] Fortunately, the MP API provides a classification of whether a material is magnetic by considering multiple states of magnetism, including ferromagnetism, antiferromagnetism, and other magnetic phases. By training the model using this classification label instead of using a cutoff value for the magnetic moment, the model's accuracy improves and reaches 93.33%. Again, we apply transfer learning to train the model on classifying the monolayers in C2DB into magnetic or nonmagnetic, reaching an accuracy of 93.33% on C2DB. The performance of both the classification and regression models with and without the use of transfer learning is compared in Table 1. An early stopping condition was set to activate after 15 epochs without improvement on the validation data. As shown by Table 1, models utilizing transfer learning met this condition more quickly but interestingly, did not improve the accuracy score. Additionally, the E_{hull} regression model achieves better performance in fewer epochs.

To demonstrate the model's robust performance in classifying magnetic materials across different symmetries, we present the model's accuracy among the space groups in the testing data in Figure 5. As shown, the model's accuracy is high across the majority of the space groups in the test data.

Lattice Relaxation through M3GNet IAP. The M3GNet IAP is a GNN-based approach using IAPs that predicts the energies, forces, and stresses of a material.[56] To find the energetic minima, we used this model to relax the crystal shape by applying in-plane strain on the lattice. Then, the predicted energies are fitted to the volumes using the stabilized jellium equation of state provided through the atomic simulation environment.[87,88] A visualization of the fitting process, as strain is exerted on a monolayer of Au_3Br_2SSe from the C2DB (ID = 4605), is presented in Figure 6.

To evaluate the efficacy of this model at performing symmetry-constrained relaxation, we employed the 2-norm difference between the symmetry-constrained IAP relaxation and DFT relaxed lattice vector matrices. For a given material, this is computed as $\|\mathbf{A}_{IAP} - \mathbf{A}_{DFT}\|_2$, where $\mathbf{A}_{IAP}$ and $\mathbf{A}_{DFT}$ are the respective lattice vector matrices. For a given set of materials, the average 2-norm difference is given by $\bar{D} = \frac{1}{N}\sum_{i=1}^{N} \|\mathbf{A}_{IAP,i} - \mathbf{A}_{DFT,i}\|_2$, where N is the total number of materials. This average $\bar{D}$ provides a statistical measure of the IAP method's accuracy in reproducing DFT-computed lattice parameters across a variety of materials. By computing the average 2-norm difference across all entries in C2DB, we obtained a value of $\bar{D}$ = 0.19 Å. This result demonstrates that through the utilization of ML, M3GNet IAPs are capable of

https://doi.org/10.1021/acs.jpcc.3c07246
J. Phys. Chem. C 2024, 128, 6007−6018

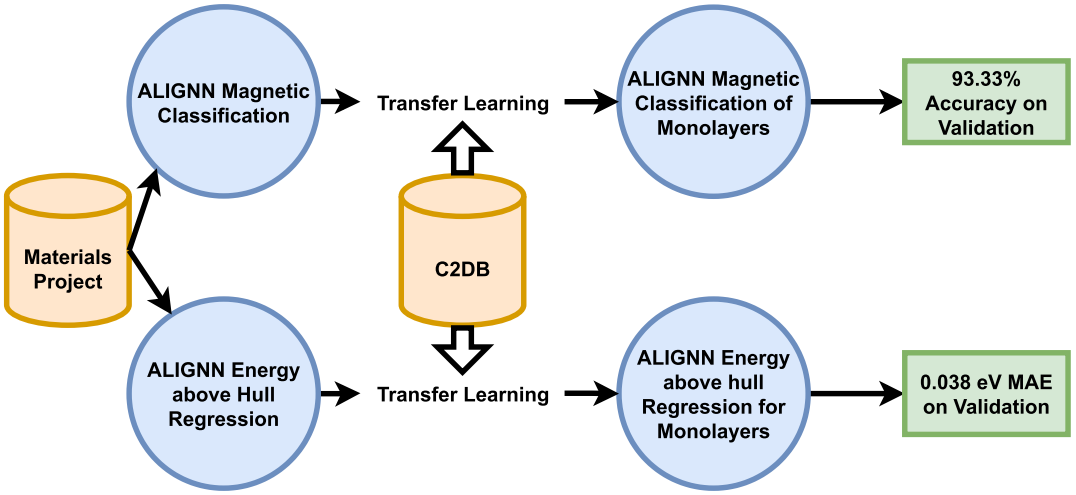

Figure 4. Outline of training CDVAE to generate 11,100 candidate monolayers for further screening.

Table 1. Effect of Transfer Learning on Performance on the Test Dataset and the Speed of Training

	magnetic classification		E_{hull} regression	
	training epochs	accuracy	training epochs	MAE
with transfer learning	18	93.33	159	0.044
without transfer learning	32	93.33	169	0.039

achieving near-DFT performance levels at a significantly reduced computational cost. For comparison, the default pretrained ALIGNN-FF model achieves $\overline{D}$ = 0.47 Å. The result of the symmetry-constrained relaxation fit using ALIGNN-FF is shown in the Supporting Information in Figure S2.

Screening and DFT Calculations. Now that all of the necessary components for generating, screening, and symmetry relaxation have been developed, we integrate them into a single pipeline, as shown in Figure 7.

After the monolayer candidates are generated by CDVAE, they are passed through a screening step. The trained ALIGNN discriminator models are then used to make predictions on the generated monolayers. We keep only monolayers where the classification model outputs a 95% probability of being magnetic and the regression model predicts the value of $E_{hull} \leq 0.3$ eV/atom. We also check for charge neutrality and run electronegativity tests as implemented in the Semiconducting Materials from Analogy and Chemical Theory (SMACT) Python library.[89]

Additionally, by constraining the number of atoms in the crystal to 5 or less, we further refined the candidate pool to the order of hundreds. This value was chosen because it loosely aligns with the 25-percentile value of the number of atoms in the magnetic monolayers in C2DB, as shown in Figure S1. Using a smaller number of atoms allows us to perform less

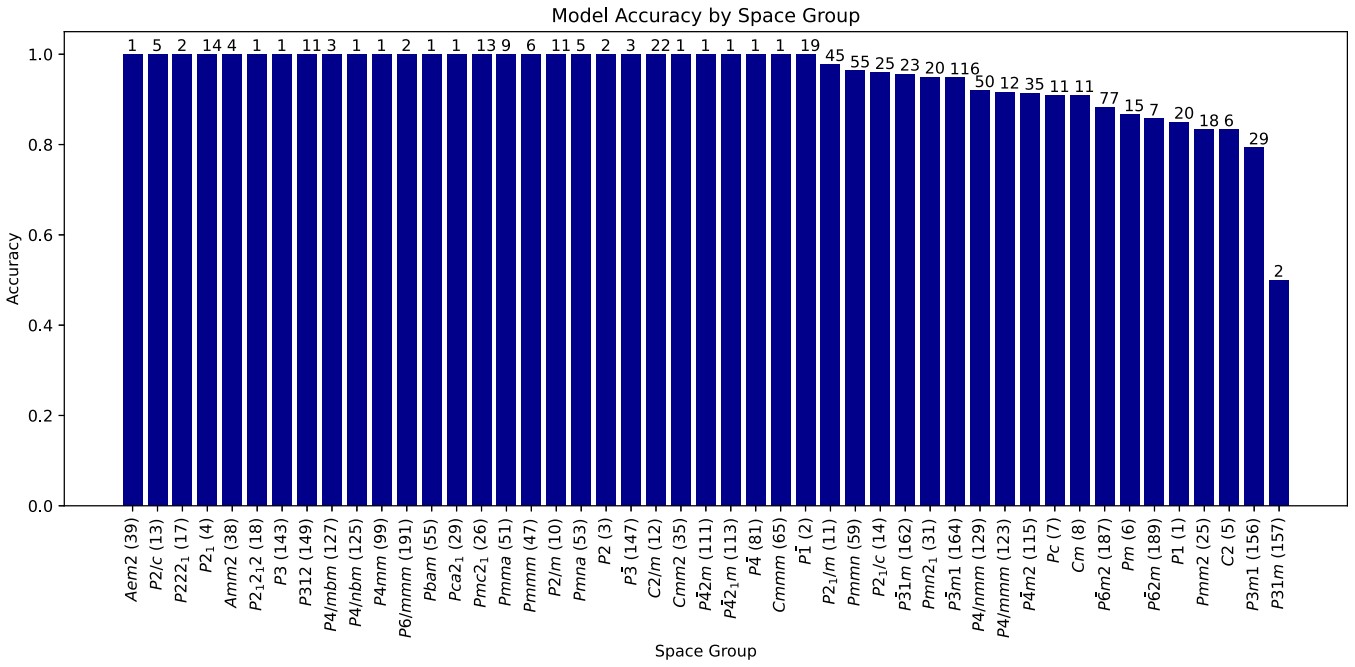

Figure 5. Model accuracy across different space groups in the test data; the number of test data points from each group is indicated on each bin.

https://doi.org/10.1021/acs.jpcc.3c07246
J. Phys. Chem. C 2024, 128, 6007−6018

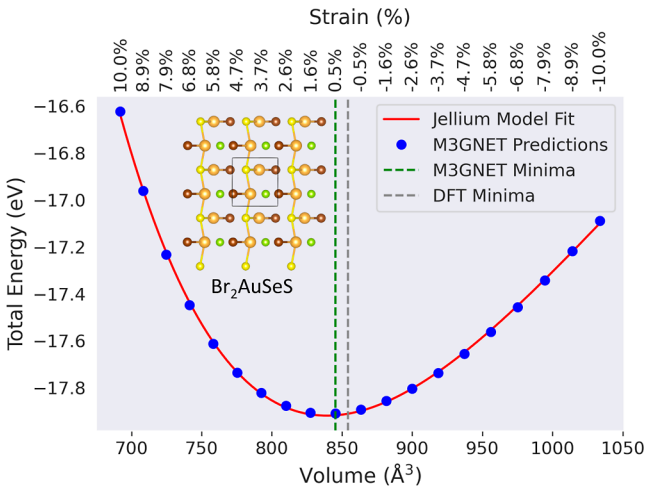

Figure 6. Symmetry-constrained relaxation by applying strain fitted to the jellium model. Energetic minima obtained using DFT and M3GNet are indicated in the plot.

computationally expensive calculations, given that DFT methods typically scale as $O(N^3)$, where N is the number of atoms.[90] Duplicate materials were removed by comparing the stoichiometries to the entries available in C2DB. Finally, we implement a dimensionality check step based on covalently bonded clusters to determine the dimensions of connected subunits in a structure, implemented in the Python materials genomic (Pymatgen) library.[91,92]

After screening, we identified 190 nonduplicate candidates compared to C2DB. This relatively large number of candidates highlights CDVAE's ability to generate new materials, especially when considering that more than 3000 materials in the database have been added to the database by a CDVAE model. This potentially indicates that CDVAE models are capable of generating new materials from unexplored chemical spaces by simply adjusting the training data to include examples that are representative of the desired properties.

Additionally, only four of these materials out of the 1100 materials were generated through optimization for the energy above the convex hull in latent space. All other materials were generated without optimization for any properties in the latent space. It may be that allowing the diffusion model to explore the chemical space without trying to optimize for a property in the latent space could allow for more diverse material generation. Since materials in the training data have low energies above the convex hull, this property is inherited in the generated crystals. Interestingly, thousands of materials added to the C2DB by a CDVAE model were generated without any optimization of energies above the convex hull.

Proceeding with our workflow, we performed IAP symmetry-constrained optimizations of these crystals, followed by DFT relaxations and self-consistent calculations. The relaxed structures are then further screened through four different, independent tests to exclude materials that did not relax into 2D structures.[93−95] In this step, a structure is considered to be 2D only if all four-dimensionality tests have been passed. This reduces the total number of materials considered in this work to a final count of 173 all of which belonged to the P1 space group. The low-symmetry of the generated structures is consistent with the reported low-symmetry in other works, indicating a pitfall of CDVAE.[60,62]

After checking C2DB, MP database, JARVIS, and OQMD for the presence of generated materials by querying the Open Databases Integration for Materials Design (OPTIMADE),[96] 130 of the generated materials were deemed to be unreported as bulk or 2D. The rest of the materials were reported across the three databases we queried, with the majority being reported in OQMD. We have listed all the generated chemical formulas in our work and their matches in the other databases, including the space groups in the Supporting Information.

The formation energy per atom, E_f, for each structure was computed using the formula: $E_f = \frac{E_{total} - \sum_i n_i E_i}{N}$, where E_{total} is

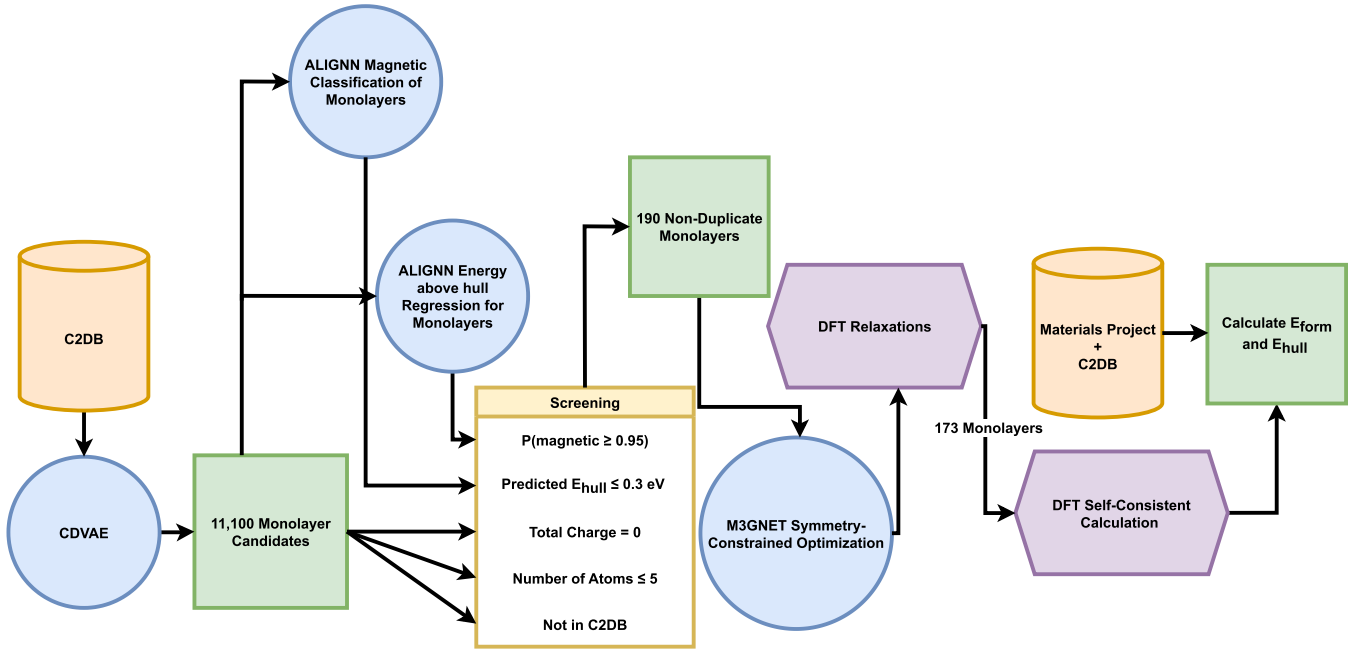

Figure 7. Full data pipeline of material generation, screening, and DFT calculations.

https://doi.org/10.1021/acs.jpcc.3c07246
J. Phys. Chem. C 2024, 128, 6007−6018

the total energy of the structure (obtained for DFT), n_i is the number of atoms of element i in the structure, E_i is the energy of element i obtained from the MP database, and N is the total number of atoms in the structure.

In C2DB, the energy above the convex hull is constructed by considering the formation energy of elementary, binary, and ternary bulk crystals in OQMD.[5,6] Naturally, this limits the number of considered phases and excludes 2D materials from competing phases. To expand the scope of the considered competing phases, we have computed the energy above the convex hull using the formation energies of compounds available in the MP database and C2DB without any restriction on the number of constituent elements. For competing phases in the MP database, only entries computed with GGA functionals and without the inclusion of a Hubbard U parameter were considered to ensure the exclusion of any energetic inconsistencies that may arise from the employing of different U values. The distribution of the E_{hull} of the monolayers generated through this pipeline is shown in Figure 8. Of the generated monolayers, 91 achieved an E_{hull} of 0, while 171 displayed an $E_{hull} \leq 0.3$ eV/atom. It is worth noting that only two materials were found to have $E_{hull} > 0.3$.

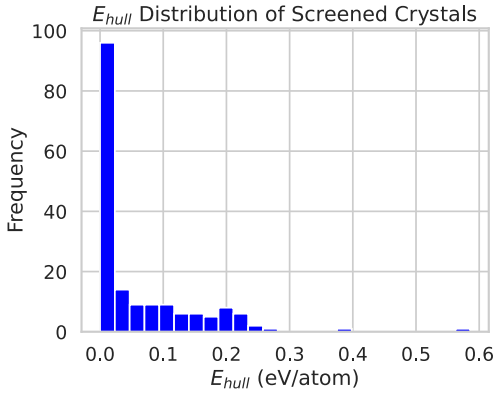

Figure 8. Distribution of E_{hull} of 173 final monolayers generated by the pipeline.

While the energy above the convex hull provides a theoretical assessment of thermodynamic stability, materials with energies above the convex hull may be experimentally realizable for many reasons. First, PBE functionals deviate from experimental values of formation energies by ≈0.25 ev/atom, which in turn affects the accuracy of the energy above the convex hull predictions.[97] Second, the monolayers generated herein are being proposed as freestanding monolayers and ignore external interactions with the environment, such as substrate effects that may stabilize these monolayers. For example, silicene has a formation energy of 0.66 eV/atom[5] but can be synthesized on a metal substrate.[98,99] Moreover, even materials such as MoS_2 and ZrS_2 with $E_{hull} > 0$ have been experimentally synthesized.[5,98] In fact, based on the hull energies of 55 experimentally observed 2D materials, the criterion for high thermodynamical stability of 2D materials was proposed to be $E_{hull} \leq 0.2$ eV/atom[5] for calculations performed using PBE functionals. This criterion has been adopted in first-principle calculations to perform a screening of 2D materials suitable for photoelectrocatalytic water splitting.[13]

In addition to thermodynamic stability, mechanical and dynamical stabilities are also necessary for the realization of 2D materials. Dynamical stability can be assessed through the absence of imaginary modes in the phonon band dispersions of materials. We used the small-displacements method, implemented in the Phonopy software package,[100] to calculate the phonon band dispersions of the 6 materials shown in Figure 9. These materials have been confirmed to be magnetic and have $E_{hull} = 0$. Two of these materials, $MnGaClO_2$ and V_2SBr_2, display no imaginary phonon modes and therefore are dynamically stable. The phonon band dispersions of Mn_2ISBr and MnGaSeSI show slightly imaginary phonon modes near the Γ point, but are likely dynamically stable. Such slight imaginary modes have been reported in DFT-calculated phonon dispersions of many 2D materials, including experimentally realized ones such as GaSe and have been attributed to interactions between periodic monolayer images and numerical instabilities.[101−104] These small imaginary modes occur at the long-wavelength limit, typically in the acoustic branch possessing the lowest frequency near the Γ point; we have highlighted this acoustic phonon branch in red for both materials. To the best of our knowledge, these four

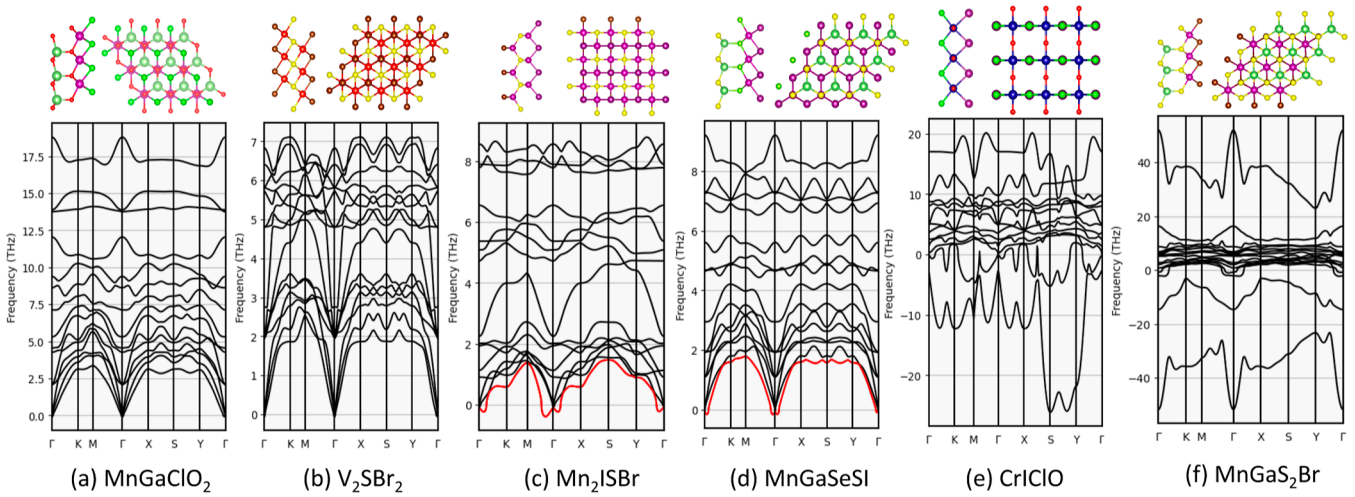

Figure 9. Phonon band dispersions of 6 materials generated through our workflow; (a) and (b) are dynamically stable, (c) and (d) are likely stable, while (e) and (f) are likely unstable. Top and side view of the generated crystals are shown atop each subfigure to the right and left, respectively.

https://doi.org/10.1021/acs.jpcc.3c07246
J. Phys. Chem. C 2024, 128, 6007−6018

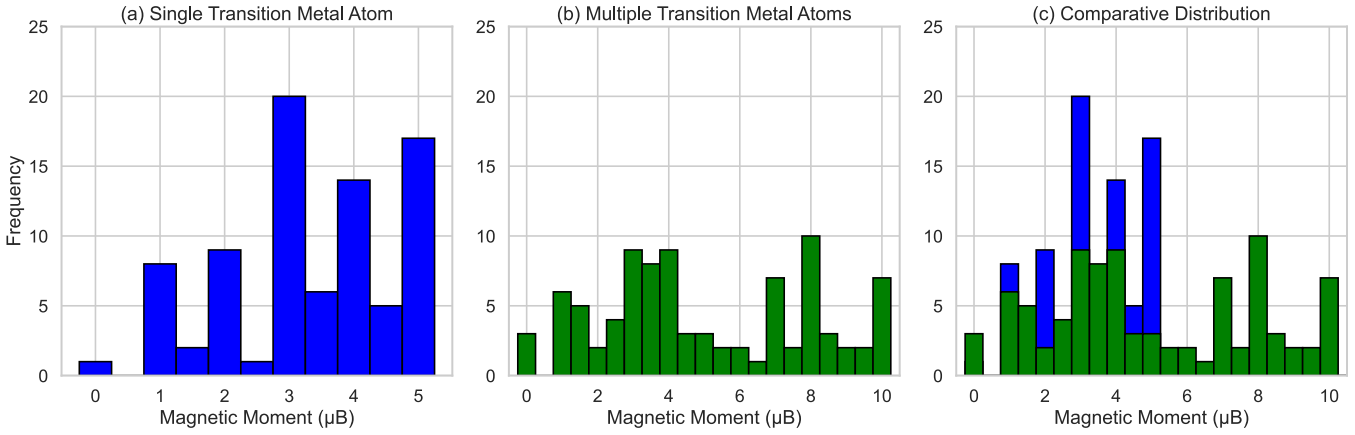

Figure 10. (a) Distribution of the total magnetic moment when a single transition metal atom exists shows peaks at integer values. (b) Distribution of magnetic moments with more than one transient metal atom exhibits a wide range of values. (c) Combined histogram displaying both magnetic moment distributions.

likely stable crystals have not been reported in bulk or as monolayers in any database at the time of writing.

The last two crystals of MnSeS and CrIClO exhibit large imaginary phonon modes and are likely unstable. Large negative phonon modes typically indicate dynamic instabilities in the structure. However, they may also indicate that the crystal is on the verge of structural transitions or distortions, such as the formation of phases hosting a charge density wave (CDW).[105] For example, MoS_2 undergoes a transition from 1T to 1T′ through a 2×1 distorted structure.[106,107] Furthermore, many transition metal dichalcogenide monolayers undergo a transition to a CDW, including $NbSe_2$,[108] TaS_2,[109] $TaSe_2$,[110] $TiSe_2$,[111] VS_2,[112] and $NbTe_2$.[113] Moreover, a transition to a CDW has been theoretically predicted for the $CrTe_2$ monolayer and was shown to stabilize the imaginary phonon modes through crystal by a transition to a $\sqrt{3} \times \sqrt{3}$ supercell.[114] In fact, because these transitions typically require the construction of supercells capable of accommodating the onset of the new phase, one of the approaches to stabilizing such materials is to extend the atoms along the direction of instability. This approach has been utilized as the basis for a high-throughput DFT study to stabilize monolayers that exhibit structural instabilities in C2DB.[12] Finally, accounting for strong electron correlations through a Hubbard U as low as 1 eV has been found to stabilize the imaginary phonon modes in 1T-$CrTe_2$.[115] However, considering the aforementioned approaches to stabilizing the materials generated here go beyond the scope of this work; our aim is to provide motivation and a blueprint for accelerating the discovery and screening of materials with specified properties.

Of the materials analyzed, only two demonstrated a total magnetic moment less than 0.5 μ_B. On average, materials exhibited a magnetic moment of 4.21 μ_B. The distribution of the DFT calculated magnetic moments is shown in Figure 10. In (a), we have binned the total magnetic moments of crystals containing only a single transition metal atom. Clearly, the magnetic moments from the screened structures exhibit prominent peaks at integer values, suggesting a strong correlation with atomic electronic configurations. Notably, while peaks can be observed at the bins representing integer values, any data points are absent at 6 and 7 μ_B since configurations with 6 or 7 unpaired electrons are not achievable in a true ground state. As crystals with more magnetic moments are considered (b), we observe an increase of the total magnetization to ≈5 μ_B and climbing to ≈10 μ_B. Because the considered materials contain at most two transition metal atoms, these large values have likely been produced by two magnetic atoms, each possessing a magnetic moment of ≈5 μ_B.

The pattern largely aligns with the behavior of the individual magnetic atoms. This consistency is observed in the majority of the screened structures, where we constrained the number of atoms to five or less and most compounds featured just one magnetic element. This dataset accentuates the intricate relationship between atomic configurations and resultant magnetic moments, particularly when compounds comprise multiple magnetic atoms.

Overall, from the 190 materials with which we performed DFT calculations, 173 were truly 2D. Of those 173, two materials possessed $E_{hull} > 0.3$ eV/atom, and four materials displayed a total magnetic moment of less than 0.5 μ_B. This demonstrates the CDVAE's capability to generate realistic structures and underscores the efficiency of the discriminator ALIGNN models in learning the underlying distributions of the energy above the convex hull and magnetism.

We have made the monolayer data available at (https://github.com/rashigeek/2D-mag-GNN including the structure of all 173 monolayers). The GitHub repository also contains the code used to produce the results. Additionally, we have provided a complete table of each material, its magnetic moment, and the energy above the convex hull in the Supporting Information.

CONCLUSIONS

In this study, we presented an integrated computational approach that combines deep learning, symmetry-constrained optimizations, and DFT calculations to generate and screen potential 2D magnetic materials. The process begins with the generation of candidate monolayers by using the CDVAE model. Candidates are then rigorously screened based on magnetic probability and thermal stability predictions from trained ALIGNN discriminator models. Screened candidates undergo lattice relaxation using the M3GNet IAP, with the final properties computed using DFT.

Our findings demonstrate that the proposed pipeline is effective in predicting magnetic, thermodynamically stable monolayers. The observed distributions of magnetic moments and energies above the convex hull provide a deeper

https://doi.org/10.1021/acs.jpcc.3c07246
J. Phys. Chem. C 2024, 128, 6007−6018

understanding of the interplay between atomic configurations and magnetic properties, revealing distinct patterns and behaviors. By integrating ML and traditional computational techniques, we can expedite the discovery process, paving the way for next-generation materials with properties tailored to specific applications. Moreover, due to the multitude of properties that can also be analyzed using a similar approach to what we have discussed, our work presents a guideline on how to accelerate inverse-design material generation for optimized properties.

■ ASSOCIATED CONTENT

Supporting Information

The Supporting Information is available free of charge at https://pubs.acs.org/doi/10.1021/acs.jpcc.3c07246.

Histogram of the number of atoms in magnetic monolayer entries in C2DB, generated monolayers, magnetic moments, energies above the convex hull, and presence in OQMD, MP, C2DB, or JARVIS (PDF)

■ AUTHOR INFORMATION

Corresponding Authors

Ahmed Elrashidy − *Department of Physics, Astronomy, and Geosciences, Towson University, Towson, Maryland 21252, United States;* orcid.org/0009-0007-1909-9345; Email: aalras2@students.towson.edu

Jia-An Yan − *Department of Physics, Astronomy, and Geosciences, Towson University, Towson, Maryland 21252, United States*; Email: jyan@towson.edu

Author

James Della-Giustina − *Department of Mathematics, Towson University, Towson, Maryland 21252, United States*

Complete contact information is available at: https://pubs.acs.org/10.1021/acs.jpcc.3c07246

Notes

The authors declare no competing financial interest.

■ ACKNOWLEDGMENTS

The authors thank Kristian Sommer Thygesen for kindly providing the C2DB. Ahmed E. would also like to thank Ryan Paxson for valuable discussions. This work used EXPANSE at the San Diego Supercomputing Center (SDSC) through allocation PHY220161 from the Advanced Cyberinfrastructure Coordination Ecosystem: Services & Support (ACCESS) program. We acknowledge support from the NSF grant DMR 1709781 and support from the Fisher General Endowment and SET grants from the Jess and Mildred Fisher College of Science and Mathematics at Towson University.

■ REFERENCES

(1) Jain, A.; Ong, S. P.; Hautier, G.; Chen, W.; Richards, W. D.; Dacek, S.; Cholia, S.; Gunter, D.; Skinner, D.; Ceder, G.; Persson, K. A. Commentary: the Materials Project: a materials genome approach to accelerating materials innovation. *APL Mater.* **2013**, *1*, 011002.

(2) Choudhary, K.; Garrity, K. F.; Reid, A. C.; DeCost, B.; Biacchi, A. J.; Hight Walker, A. R.; Trautt, Z.; Hattrick-Simpers, J.; Kusne, A. G.; Centrone, A.; et al. The joint automated repository for various integrated simulations (JARVIS) for data-driven materials design. *npj Comput. Mater.* **2020**, *6*, 173.

(3) Saal, J. E.; Kirklin, S.; Aykol, M.; Meredig, B.; Wolverton, C. Materials design and discovery with high-throughput density functional theory: the open quantum materials database (OQMD). *JOM* **2013**, *65*, 1501−1509.

(4) Kirklin, S.; Saal, J. E.; Meredig, B.; Thompson, A.; Doak, J. W.; Aykol, M.; Rühl, S.; Wolverton, C. The open quantum materials database (OQMD): assessing the accuracy of DFT formation energies. *npj Comput. Mater.* **2015**, *1*, 15010.

(5) Haastrup, S.; Strange, M.; Pandey, M.; Deilmann, T.; Schmidt, P. S.; Hinsche, N. F.; Gjerding, M. N.; Torelli, D.; Larsen, P. M.; Riis-Jensen, A. C.; et al. The computational 2D materials database: high-throughput modeling and discovery of atomically thin crystals. *2D Mater.* **2018**, *5*, 042002.

(6) Gjerding, M. N.; Taghizadeh, A.; Rasmussen, A.; Ali, S.; Bertoldo, F.; Deilmann, T.; Knøsgaard, N. R.; Kruse, M.; Larsen, A. H.; Manti, S.; et al. Recent progress of the computational 2D materials database (C2DB). *2D Mater.* **2021**, *8*, 044002.

(7) Moustafa, H.; Larsen, P. M.; Gjerding, M. N.; Mortensen, J. J.; Thygesen, K. S.; Jacobsen, K. W. Computational exfoliation of atomically thin one-dimensional materials with application to Majorana bound states. *Phys. Rev. Mater.* **2022**, *6*, 064202.

(8) Butler, K. T.; Davies, D. W.; Cartwright, H.; Isayev, O.; Walsh, A. Machine learning for molecular and materials science. *Nature* **2018**, *559*, 547−555.

(9) Zuo, Y.; Qin, M.; Chen, C.; Ye, W.; Li, X.; Luo, J.; Ong, S. P. Accelerating materials discovery with Bayesian optimization and graph deep learning. *Mater. Today* **2021**, *51*, 126−135.

(10) Pant, D.; Pokharel, S.; Mandal, S.; Kc, D. B.; Pati, R. DFT-aided machine learning-based discovery of magnetism in Fe-based bimetallic chalcogenides. *Sci. Rep.* **2023**, *13*, 3277.

(11) Ibrahim, A.; Wines, D.; Ataca, C. Modeling Chemical Exfoliation of Non-van der Waals Chromium Sulfides by Machine Learning Interatomic Potentials and Monte Carlo Simulations. *J. Phys. Chem. C* **2024**, *128* (3), 1267−1283.

(12) Manti, S.; Svendsen, M. K.; Knøsgaard, N. R.; Lyngby, P. M.; Thygesen, K. S. Exploring and machine learning structural instabilities in 2D materials. *npj Comput. Mater.* **2023**, *9*, 33.

(13) Schleder, G. R.; Acosta, C. M.; Fazzio, A. Exploring two-dimensional materials thermodynamic stability via machine learning. *ACS Appl. Mater. Interfaces* **2020**, *12*, 20149−20157.

(14) Sorkun, M. C.; Astruc, S.; Koelman, J. M. V. A.; Er, S. An artificial intelligence-aided virtual screening recipe for two-dimensional materials discovery. *npj Comput. Mater.* **2020**, *6*, 106.

(15) Wang, H.-C.; Schmidt, J.; Marques, M. A.; Wirtz, L.; Romero, A. H. Symmetry-based computational search for novel binary and ternary 2D materials. *2D Mater.* **2023**, *10*, 035007.

(16) Wines, D.; Choudhary, K.; Biacchi, A. J.; Garrity, K. F.; Tavazza, F. High-throughput DFT-based discovery of next generation two-dimensional (2D) superconductors. *Nano Lett.* **2023**, *23*, 969−978.

(17) Mermin, N. D.; Wagner, H. Absence of ferromagnetism or antiferromagnetism in one-or two-dimensional isotropic Heisenberg models. *Phys. Rev. Lett.* **1966**, *17*, 1133−1136.

(18) Lee, J.-U.; Lee, S.; Ryoo, J. H.; Kang, S.; Kim, T. Y.; Kim, P.; Park, C.-H.; Park, J.-G.; Cheong, H. Ising-type magnetic ordering in atomically thin $FePS_3$. *Nano Lett.* **2016**, *16*, 7433−7438.

(19) Huang, B.; Clark, G.; Navarro-Moratalla, E.; Klein, D. R.; Cheng, R.; Seyler, K. L.; Zhong, D.; Schmidgall, E.; McGuire, M. A.; Cobden, D. H.; et al. Layer-dependent ferromagnetism in a van der Waals crystal down to the monolayer limit. *Nature* **2017**, *546*, 270−273.

(20) Gong, C.; Li, L.; Li, Z.; Ji, H.; Stern, A.; Xia, Y.; Cao, T.; Bao, W.; Wang, C.; Wang, Y.; et al. Discovery of intrinsic ferromagnetism in two-dimensional van der Waals crystals. *Nature* **2017**, *546*, 265−269.

(21) Fei, Z.; Huang, B.; Malinowski, P.; Wang, W.; Song, T.; Sanchez, J.; Yao, W.; Xiao, D.; Zhu, X.; May, A. F.; et al. Two-dimensional itinerant ferromagnetism in atomically thin Fe_3GeTe_2. *Nat. Mater.* **2018**, *17*, 778−782.

(22) Zhang, Z.; Shang, J.; Jiang, C.; Rasmita, A.; Gao, W.; Yu, T. Direct photoluminescence probing of ferromagnetism in monolayer two-dimensional $CrBr_3$. *Nano Lett.* **2019**, *19*, 3138−3142.
(23) Kumari, S.; Pradhan, D. K.; Pradhan, N. R.; Rack, P. D. Recent developments on 2D magnetic materials: challenges and opportunities. *Emergent Mater.* **2021**, *4*, 827−846.
(24) Zhao, B.; Ngaloy, R.; Ghosh, S.; Ershadrad, S.; Gupta, R.; Ali, K.; Hoque, A. M.; Karpiak, B.; Khokhriakov, D.; Polley, C.; et al. A room-temperature spin-valve with van der Waals ferromagnet Fe_5GeTe_2/graphene heterostructure. *Adv. Mater.* **2023**, *35*, 2209113.
(25) Wu, H.; Zhang, W.; Yang, L.; Wang, J.; Li, J.; Li, L.; Gao, Y.; Zhang, L.; Du, J.; Shu, H.; et al. Strong intrinsic room-temperature ferromagnetism in freestanding non-van der Waals ultrathin 2D crystals. *Nat. Commun.* **2021**, *12*, 5688.
(26) Zhao, Z.; Zhou, J.; Liu, L.; Liu, N.; Huang, J.; Zhang, B.; Li, W.; Zeng, Y.; Zhang, T.; Ji, W.; et al. Two-dimensional room-temperature magnetic nonstoichiometric Fe_7Se_8 nanocrystals: controllable synthesis and magnetic behavior. *Nano Lett.* **2022**, *22*, 1242−1250.
(27) Zhang, G.; Guo, F.; Wu, H.; Wen, X.; Yang, L.; Jin, W.; Zhang, W.; Chang, H. Above-room-temperature strong intrinsic ferromagnetism in 2D van der Waals Fe_3GaTe_2 with large perpendicular magnetic anisotropy. *Nat. Commun.* **2022**, *13*, 5067.
(28) Cai, L.; Tung, V.; Wee, A. Room-temperature ferromagnetism in two-dimensional transition metal chalcogenides: strategies and origin. *J. Alloys Compd.* **2022**, *913*, 165289.
(29) Zhang, X.; Lu, Q.; Liu, W.; Niu, W.; Sun, J.; Cook, J.; Vaninger, M.; Miceli, P. F.; Singh, D. J.; Lian, S.-W.; et al. Room-temperature intrinsic ferromagnetism in epitaxial $CrTe_2$ ultrathin films. *Nat. Commun.* **2021**, *12*, 2492.
(30) Liu, P.; Zhang, Y.; Li, K.; Li, Y.; Pu, Y. Recent advances in 2D van der Waals magnets: detection, modulation, and applications. *iScience* **2023**, *26*, 107584.
(31) Lee, Y. H. Is it possible to create magnetic semiconductors that function at room temperature? *Science* **2023**, *382*, No. eadl0823.
(32) Ontoso, N.; Safeer, C.; Herling, F.; Ingla-Aynés, J.; Yang, H.; Chi, Z.; Martin-Garcia, B.; Robredo, I.; Vergniory, M. G.; De Juan, F.; et al. Unconventional charge-to-spin conversion in graphene/$MoTe_2$ van der Waals heterostructures. *Phys. Rev. Appl.* **2023**, *19*, 014053.
(33) Shaginyan, V. R.; Stephanovich, V.; Msezane, A.; Japaridze, G.; Clark, J.; Amusia, M. Y.; Kirichenko, E. Theoretical and experimental developments in quantum spin liquid in geometrically frustrated magnets: a review. *J. Mater. Sci.* **2020**, *55*, 2257−2290.
(34) Banerjee, A.; Bridges, C.; Yan, J.-Q.; Aczel, A.; Li, L.; Stone, M.; Granroth, G.; Lumsden, M.; Yiu, Y.; Knolle, J.; et al. Proximate Kitaev quantum spin liquid behaviour in a honeycomb magnet. *Nat. Mater.* **2016**, *15*, 733−740.
(35) Sachs, B.; Wehling, T.; Novoselov, K.; Lichtenstein, A.; Katsnelson, M. Ferromagnetic two-dimensional crystals: single layers of K_2CuF_4. *Phys. Rev. B* **2013**, *88*, 201402.
(36) Han, M.-G.; Garlow, J. A.; Liu, Y.; Zhang, H.; Li, J.; DiMarzio, D.; Knight, M. W.; Petrovic, C.; Jariwala, D.; Zhu, Y. Topological magnetic-spin textures in two-dimensional van der Waals $Cr_2Ge_2Te_6$. *Nano Lett.* **2019**, *19*, 7859−7865.
(37) Khela, M.; Dąbrowski, M.; Khan, S.; Keatley, P. S.; Verzhbitskiy, I.; Eda, G.; Hicken, R. J.; Kurebayashi, H.; Santos, E. J. Laser-induced topological spin switching in a 2D van der Waals magnet. *Nat. Commun.* **2023**, *14*, 1378.
(38) Zhang, X.; Wang, X.; He, T.; Wang, L.; Yu, W.-W.; Liu, Y.; Liu, G.; Cheng, Z. Magnetic topological materials in two-dimensional: theory, material realization and application prospects. *Sci. Bull.* **2023**, *68*, 2639−2657.
(39) Zhu, Y.; Kong, X.; Rhone, T. D.; Guo, H. Systematic search for two-dimensional ferromagnetic materials. *Phys. Rev. Mater.* **2018**, *2*, 081001.
(40) Wang, Y.; Kajihara, S.; Matsuoka, H.; Saika, B. K.; Yamagami, K.; Takeda, Y.; Wadati, H.; Ishizaka, K.; Iwasa, Y.; Nakano, M. Layer-number-independent two-dimensional ferromagnetism in Cr_3Te_4. *Nano Lett.* **2022**, *22*, 9964−9971.
(41) Torelli, D.; Moustafa, H.; Jacobsen, K. W.; Olsen, T. High-throughput computational screening for two-dimensional magnetic materials based on experimental databases of three-dimensional compounds. *npj Comput. Mater.* **2020**, *6*, 158.
(42) Horton, M. K.; Montoya, J. H.; Liu, M.; Persson, K. A. High-throughput prediction of the ground-state collinear magnetic order of inorganic materials using density functional theory. *npj Comput. Mater.* **2019**, *5*, 64.
(43) Choudhary, K.; Garrity, K. F.; Jiang, J.; Pachter, R.; Tavazza, F. Computational search for magnetic and non-magnetic 2D topological materials using unified spin−orbit spillage screening. *npj Comput. Mater.* **2020**, *6*, 49.
(44) Minch, P.; Bhattarai, R.; Rhone, T. D. Data-driven study of magnetic anisotropy in transition metal dichalcogenide monolayers. *Solid State Commun.* **2023**, *371*, 115248.
(45) Torelli, D.; Thygesen, K. S.; Olsen, T. High throughput computational screening for 2D ferromagnetic materials: the critical role of anisotropy and local correlations. *2D Mater.* **2019**, *6*, 045018.
(46) Xie, Y.; Tritsaris, G. A.; Granas, O.; Rhone, T. D. Data-driven studies of the magnetic anisotropy of two-dimensional magnetic materials. *J. Phys. Chem. Lett.* **2021**, *12*, 12048−12054.
(47) Rhone, T. D.; Bhattarai, R.; Gavras, H.; Lusch, B.; Salim, M.; Mattheakis, M.; Larson, D. T.; Krockenberger, Y.; Kaxiras, E. Artificial intelligence guided studies of van der Waals magnets. *Adv. Theory Simul.* **2023**, *6*, 2300019.
(48) Rhone, T. D.; Chen, W.; Desai, S.; Torrisi, S. B.; Larson, D. T.; Yacoby, A.; Kaxiras, E. Data-driven studies of magnetic two-dimensional materials. *Sci. Rep.* **2020**, *10*, 15795.
(49) Bhattarai, R.; Minch, P.; Rhone, T. D. Investigating magnetic van der Waals materials using data-driven approaches. *J. Mater. Chem. C* **2023**, *11*, 5601−5610.
(50) Chen, T.; Guestrin, C. XGBoost: a scalable tree boosting system. In *Proceedings of the 22nd ACM SIGKDD International Conference on Knowledge Discovery and Data Mining. New York, NY, USA*, 2016; pp 785−794.
(51) Acosta, C. M.; Ogoshi, E.; Souza, J. A.; Dalpian, G. M. Machine learning study of the magnetic ordering in 2D materials. *ACS Appl. Mater. Interfaces* **2022**, *14*, 9418−9432.
(52) Zhou, J.; Cui, G.; Hu, S.; Zhang, Z.; Yang, C.; Liu, Z.; Wang, L.; Li, C.; Sun, M. Graph neural networks: a review of methods and applications. *AI Open* **2020**, *1*, 57−81.
(53) Reiser, P.; Neubert, M.; Eberhard, A.; Torresi, L.; Zhou, C.; Shao, C.; Metni, H.; van Hoesel, C.; Schopmans, H.; Sommer, T.; Friederich, P. Graph neural networks for materials science and chemistry. *Commun. Mater.* **2022**, *3*, 93.
(54) Xie, T.; Fu, X.; Ganea, O.-E.; Barzilay, R.; Jaakkola, T. S. Crystal diffusion variational autoencoder for periodic material generation. In *International Conference on Learning Representations*, 2022.
(55) Choudhary, K.; DeCost, B. Atomistic line graph neural network for improved materials property predictions. *npj Comput. Mater.* **2021**, *7*, 185.
(56) Chen, C.; Ong, S. P. A universal graph deep learning interatomic potential for the periodic table. *Nat. Comput. Sci.* **2022**, *2*, 718−728.
(57) Sohl-Dickstein, J.; Weiss, E.; Maheswaranathan, N.; Ganguli, S. Deep unsupervised learning using nonequilibrium thermodynamics. In *International Conference on Machine Learning*, 2015; pp 2256−2265.
(58) Song, Y.; Ermon, S. Generative modeling by estimating gradients of the data distribution. In *Advances in Neural Information Processing Systems*, 2019; Vol. *32*.
(59) Han, S.; Lee, J.; Han, S.; Moosavi, S. M.; Kim, J.; Park, C. Design of new inorganic crystals with the desired composition using deep learning. *J. Chem. Inf. Model.* **2023**, *63*, 5755−5763.
(60) Lyngby, P.; Thygesen, K. S. Data-driven discovery of 2D materials by deep generative models. *npj Comput. Mater.* **2022**, *8*, 232.
(61) Moustafa, H.; Lyngby, P. M.; Mortensen, J. J.; Thygesen, K. S.; Jacobsen, K. W. Hundreds of new, stable, one-dimensional materials

https://doi.org/10.1021/acs.jpcc.3c07246
J. Phys. Chem. C 2024, 128, 6007−6018

from a generative machine learning model. *Phys. Rev. Mater.* **2023**, *7*, 014007.
(62) Wines, D.; Xie, T.; Choudhary, K. Inverse design of next-generation superconductors using data-driven deep generative models. *J. Phys. Chem. Lett.* **2023**, *14*, 6630−6638.
(63) Siriwardane, E. M. D.; Zhao, Y.; Hu, J. Data-driven deep generative design of stable spintronic materials. *CrystEngComm* **2023**, *25*, 6017−6029.
(64) Kingma, D. P.; Welling, M. Auto-encoding variational Bayes. *arXiv* **2013**, arXiv:1312.6114.
(65) Batzner, S.; Musaelian, A.; Sun, L.; Geiger, M.; Mailoa, J. P.; Kornbluth, M.; Molinari, N.; Smidt, T. E.; Kozinsky, B. E(3)-equivariant graph neural networks for data-efficient and accurate interatomic potentials. *Nat. Commun.* **2022**, *13*, 2453.
(66) Wines, D.; Gurunathan, R.; Garrity, K. F.; DeCost, B.; Biacchi, A. J.; Tavazza, F.; Choudhary, K. Recent progress in the JARVIS infrastructure for next-generation data-driven materials design. *arXiv* **2023**, *10*, arXiv:2305.11842.
(67) Kresse, G.; Furthmüller, J. Efficient iterative schemes for ab initio total-energy calculations using a plane-wave basis set. *Phys. Rev. B* **1996**, *54*, 11169−11186.
(68) Kresse, G.; Joubert, D. From ultrasoft pseudopotentials to the projector augmented-wave method. *Phys. Rev. B* **1999**, *59*, 1758−1775.
(69) Perdew, J. P.; Burke, K.; Ernzerhof, M. Generalized gradient approximation made simple. *Phys. Rev. Lett.* **1996**, *77*, 3865−3868.
(70) Monkhorst, H. J.; Pack, J. D. Special points for Brillouin-zone integrations. *Phys. Rev. B* **1976**, *13*, 5188−5192.
(71) Dudarev, S. L.; Botton, G. A.; Savrasov, S. Y.; Humphreys, C.; Sutton, A. P. Electron-energy-loss spectra and the structural stability of nickel oxide: an LSDA + U study. *Phys. Rev. B* **1998**, *57*, 1505−1509.
(72) Anisimov, V. I.; Zaanen, J.; Andersen, O. K. Band theory and Mott insulators: Hubbard U instead of Stoner I. *Phys. Rev. B* **1991**, *44*, 943−954.
(73) Ylvisaker, E. R.; Pickett, W. E.; Koepernik, K. Anisotropy and magnetism in the LSDA + U method. *Phys. Rev. B* **2009**, *79*, 035103.
(74) Georges, A.; Kotliar, G.; Krauth, W.; Rozenberg, M. J. Dynamical mean-field theory of strongly correlated fermion systems and the limit of infinite dimensions. *Rev. Mod. Phys.* **1996**, *68*, 13−125.
(75) Foulkes, W.; Mitas, L.; Needs, R.; Rajagopal, G. Quantum Monte Carlo simulations of solids. *Rev. Mod. Phys.* **2001**, *73*, 33−83.
(76) Karp, J.; Hampel, A.; Millis, A. J. Dependence of DFT + DMFT results on the construction of the correlated orbitals. *Phys. Rev. B* **2021**, *103*, 195101.
(77) Zang, J.; Wang, J.; Cano, J.; Georges, A.; Millis, A. J. Dynamical mean-field theory of Moiré bilayer transition metal dichalcogenides: phase diagram, resistivity, and quantum criticality. *Phys. Rev. X* **2022**, *12*, 021064.
(78) Jiang, W.; Liu, Y.; Klein, A.; Wang, Y.; Sun, K.; Chubukov, A. V.; Meng, Z. Y. Monte Carlo study of the pseudogap and superconductivity emerging from quantum magnetic fluctuations. *Nat. Commun.* **2022**, *13*, 2655.
(79) Wines, D.; Tiihonen, J.; Saritas, K.; Krogel, J. T.; Ataca, C. A quantum Monte Carlo Study of the structural, energetic, and magnetic properties of two-dimensional H and T phase VSe_2. *J. Phys. Chem. Lett.* **2023**, *14*, 3553−3560.
(80) Wines, D.; Choudhary, K.; Tavazza, F. Systematic DFT + U and quantum Monte Carlo benchmark of magnetic two-dimensional (2D) CrX_3 (X = I, Br, Cl, F). *J. Phys. Chem. C* **2023**, *127*, 1176−1188.
(81) Priya, P.; Aluru, N. Accelerated design and discovery of perovskites with high conductivity for energy applications through machine learning. *npj Comput. Mater.* **2021**, *7*, 90.
(82) Choubisa, H.; Todorović, P.; Pina, J. M.; Parmar, D. H.; Li, Z.; Voznyy, O.; Tamblyn, I.; Sargent, E. H. Interpretable discovery of semiconductors with machine learning. *npj Comput. Mater.* **2023**, *9*, 117.
(83) Zhao, Y.; Siriwardane, E. M. D.; Wu, Z.; Fu, N.; Al-Fahdi, M.; Hu, M.; Hu, J. Physics guided deep learning for generative design of crystal materials with symmetry constraints. *npj Comput. Mater.* **2023**, *9*, 38.
(84) Carpenter, M.; Salje, E.; Howard, C. J. Magnetoelastic coupling and multiferroic ferroelastic/magnetic phase transitions in the perovskite $KMnF_3$. *Phys. Rev. B* **2012**, *85*, 224430.
(85) Webster, L.; Yan, J.-A. Strain-tunable magnetic anisotropy in monolayer $CrCl_3$, $CrBr_3$, and CrI_3. *Phys. Rev. B* **2018**, *98*, 144411.
(86) Hu, T.; Wan, W.; Ge, Y.; Liu, Y. Strain-tunable magnetic order and electronic structure in 2D $CrAsS_4$. *J. Magn. Magn. Mater.* **2020**, *497*, 165941.
(87) Larsen, A. H.; Mortensen, J. J.; Blomqvist, J.; Castelli, I. E.; Christensen, R.; Dułak, M.; Friis, J.; Groves, M. N.; Hammer, B.; Hargus, C.; et al. The atomic simulation environment—a Python library for working with atoms. *J. Phys.: Condens. Matter* **2017**, *29*, 273002.
(88) Alchagirov, A. B.; Perdew, J. P.; Boettger, J. C.; Albers, R.; Fiolhais, C. Reply to "Comment on 'Energy and pressure versus volume: equations of state motivated by the stabilized jellium model'". *Phys. Rev. B* **2003**, *67*, 026103.
(89) Davies, D. W.; Butler, K. T.; Jackson, A. J.; Morris, A.; Frost, J. M.; Skelton, J. M.; Walsh, A. Computational screening of all stoichiometric inorganic materials. *Chem* **2016**, *1*, 617−627.
(90) Sholl, D. S.; Steckel, J. A. *Density Functional Theory: A Practical Introduction*; John Wiley & Sons, 2022.
(91) Ong, S. P.; Richards, W. D.; Jain, A.; Hautier, G.; Kocher, M.; Cholia, S.; Gunter, D.; Chevrier, V. L.; Persson, K. A.; Ceder, G. Python materials genomics (pymatgen): a robust, open-source python library for materials analysis. *Comput. Mater. Sci.* **2013**, *68*, 314−319.
(92) Cheon, G.; Duerloo, K.-A. N.; Sendek, A. D.; Porter, C.; Chen, Y.; Reed, E. J. Data mining for new two-and one-dimensional weakly bonded solids and lattice-commensurate heterostructures. *Nano Lett.* **2017**, *17*, 1915−1923.
(93) Pan, H.; Ganose, A. M.; Horton, M.; Aykol, M.; Persson, K. A.; Zimmermann, N. E.; Jain, A. Benchmarking coordination number prediction algorithms on inorganic crystal structures. *Inorg. Chem.* **2021**, *60*, 1590−1603.
(94) Gorai, P.; Toberer, E. S.; Stevanović, V. Computational identification of promising thermoelectric materials among known quasi-2D binary compounds. *J. Mater. Chem. A* **2016**, *4*, 11110−11116.
(95) Larsen, P. M.; Pandey, M.; Strange, M.; Jacobsen, K. W. Definition of a scoring parameter to identify low-dimensional materials components. *Phys. Rev. Mater.* **2019**, *3*, 034003.
(96) Andersen, C. W.; Armiento, R.; Blokhin, E.; Conduit, G. J.; Dwaraknath, S.; Evans, M. L.; Fekete, Á.; Gopakumar, A.; Gražulis, S.; Merkys, A.; et al. OPTIMADE, an API for exchanging materials data. *Sci. Data* **2021**, *8*, 217.
(97) Pandey, M.; Jacobsen, K. W. Heats of formation of solids with error estimation: the mBEEF functional with and without fitted reference energies. *Phys. Rev. B* **2015**, *91*, 235201.
(98) Malyi, O. I.; Sopiha, K. V.; Persson, C. Energy, phonon, and dynamic stability criteria of two-dimensional materials. *ACS Appl. Mater. Interfaces* **2019**, *11*, 24876−24884.
(99) Li, G.; Zhang, Y.-Y.; Guo, H.; Huang, L.; Lu, H.; Lin, X.; Wang, Y.-L.; Du, S.; Gao, H.-J. Epitaxial growth and physical properties of 2D materials beyond graphene: from monatomic materials to binary compounds. *Chem. Soc. Rev.* **2018**, *47*, 6073−6100.
(100) Togo, A.; Chaput, L.; Tadano, T.; Tanaka, I. Implementation strategies in phonopy and phono3py. *J. Phys.: Condens. Matter* **2023**, *35*, 353001.
(101) Radescu, S.; Machon, D.; Mélinon, P. Origin of dynamical instabilities in some simulated two-dimensional materials: GaSe as a case study. *Phys. Rev. Mater.* **2019**, *3*, 074002.
(102) Ataca, C.; Sahin, H.; Ciraci, S. Stable, single-layer MX2 transition-metal oxides and dichalcogenides in a honeycomb-like structure. *J. Phys. Chem. C* **2012**, *116*, 8983−8999.

https://doi.org/10.1021/acs.jpcc.3c07246
J. Phys. Chem. C 2024, 128, 6007−6018

(103) Zheng, H.; Li, X.-B.; Chen, N.-K.; Xie, S.-Y.; Tian, W. Q.; Chen, Y.; Xia, H.; Zhang, S.; Sun, H.-B. Monolayer II-VI semiconductors: a first-principles prediction. *Phys. Rev. B* **2015**, *92*, 115307.
(104) Zólyomi, V.; Drummond, N.; Fal'Ko, V. Electrons and phonons in single layers of hexagonal indium chalcogenides from ab initio calculations. *Phys. Rev. B* **2014**, *89*, 205416.
(105) Gruner, G. *Density Waves in Solids*; CRC Press, 2018.
(106) Qian, X.; Liu, J.; Fu, L.; Li, J. Quantum spin Hall effect in two-dimensional transition metal dichalcogenides. *Science* **2014**, *346*, 1344−1347.
(107) Liu, L.; Wu, J.; Wu, L.; Ye, M.; Liu, X.; Wang, Q.; Hou, S.; Lu, P.; Sun, L.; Zheng, J.; et al. Phase-selective synthesis of 1T′ MoS_2 monolayers and heterophase bilayers. *Nat. Mater.* **2018**, *17*, 1108−1114.
(108) Xi, X.; Zhao, L.; Wang, Z.; Berger, H.; Forró, L.; Shan, J.; Mak, K. F. Strongly enhanced charge-density-wave order in monolayer $NbSe_2$. *Nat. Nanotechnol.* **2015**, *10*, 765−769.
(109) Yang, Y.; Fang, S.; Fatemi, V.; Ruhman, J.; Navarro-Moratalla, E.; Watanabe, K.; Taniguchi, T.; Kaxiras, E.; Jarillo-Herrero, P. Enhanced superconductivity upon weakening of charge density wave transport in 2H-TaS_2 in the two-dimensional limit. *Phys. Rev. B* **2018**, *98*, 035203.
(110) Ryu, H.; Chen, Y.; Kim, H.; Tsai, H.-Z.; Tang, S.; Jiang, J.; Liou, F.; Kahn, S.; Jia, C.; Omrani, A. A.; et al. Persistent charge-density-wave order in single-layer $TaSe_2$. *Nano Lett.* **2018**, *18*, 689−694.
(111) Sugawara, K.; Nakata, Y.; Shimizu, R.; Han, P.; Hitosugi, T.; Sato, T.; Takahashi, T. Unconventional charge-density-wave transition in monolayer 1T-$TiSe_2$. *ACS Nano* **2016**, *10*, 1341−1345.
(112) Van Efferen, C.; Berges, J.; Hall, J.; Van Loon, E.; Kraus, S.; Schobert, A.; Wekking, T.; Huttmann, F.; Plaar, E.; Rothenbach, N.; et al. A full gap above the Fermi level: the charge density wave of monolayer VS2. *Nat. Commun.* **2021**, *12*, 6837.
(113) Bai, Y.; Jian, T.; Pan, Z.; Deng, J.; Lin, X.; Zhu, C.; Huo, D.; Cheng, Z.; Liu, Y.; Cui, P.; et al. Realization of multiple charge-density waves in $NbTe_2$ at the monolayer limit. *Nano Lett.* **2023**, *23*, 2107−2113.
(114) Otero Fumega, A.; Phillips, J.; Pardo, V. Controlled two-dimensional ferromagnetism in 1T−$CrTe_2$: the role of charge density wave and strain. *J. Phys. Chem. C* **2020**, *124*, 21047−21053.
(115) Liu, Y.; Kwon, S.; de Coster, G. J.; Lake, R. K.; Neupane, M. R. Structural, electronic, and magnetic properties of $CrTe_2$. *Phys. Rev. Mater.* **2022**, *6*, 084004.

https://doi.org/10.1021/acs.jpcc.3c07246
J. Phys. Chem. C 2024, 128, 6007−6018